Analysis of Pedestrian Kinematics and Injury Mechanism in Real World Accidents

Daisuke Murakami, Chinmoy Pal, Yoshiko Kawabe and Tomosaburo Okabe

Abstract Post-impact pedestrian kinematics is complex and depends on various factors such as impact speed, height of the pedestrian, front-end profile of the striking vehicle and pedestrian posture, among others. The aim of this study is to investigate the main factors that determine post-crash pedestrian kinematics. A detailed study of NASS-PCDS (National Automotive Sampling System—Pedestrian Crash Data Study) showed that the vehicle–pedestrian interaction in frontal crashes can be categorized into four types. Pedestrian-vehicle size ratio and the impact speed are the two most influential factors that determine post crash pedestrian kinematics. The findings from the NASS-PCDS study were also confirmed and verified with the help of numerical simulations performed using two modified JAMA human FE models. An adult model (male, 175 cm and 72 kg) and a properly scaled child model (6 years old, 120 cm and 24.5 kg) were effectively utilized to investigate the post-crash kinematics in different conditions.

Keywords FE-analysis · Pedestrian-safety · Accident-analysis · 6-year-old(YO)-child · Postcrash-kinematics

1 Introduction

Even though the motor vehicle occupant fatalities are decreasing in many countries, the overall percentages of pedestrian casualties are increasing compared to that of vehicle occupants. Annual fatalities, for every 1,000,000 people, are 12.3 in

D. Murakami · C. Pal (✉) · Y. Kawabe · T. Okabe
Nissan Motor Company Ltd, Tokyo, Japan

Australia, 15.7 in the EC, 16.4 in the US and 21.8 in Japan. The numbers in developing countries are even higher. Mizuno et al. reported their detailed investigations of pedestrian accident databases from countries including Australia, Germany, Japan and the US (1,605 cases, 9,463 injuries, include 3,305 AIS2 +) [1]. According to their report, in one third of those cases, pedestrians are reported to have suffered injuries to their heads and/or lower extremities. Previous studies on pedestrian crash cases pointed out that the vehicle front geometry human height and human posture affect the pedestrian injury mechanism [2]. Further studies [3, 4] targeting child pedestrians' injury distribution pointed out that anthropometry influences impact kinematics. This study focuses on the leading factors affecting post-crash pedestrian movement and the injury mechanisms in relation to impact speed. Human FE model simulations were carried out to reconfirm and endorse the findings and the trends in accident analyses.

2 NASS-PCDS Analysis

The database contains data on 552 pedestrian crashes and 4,499 injuries during 1994–1998. It is not a statistically weighted sample. Statistical inferences of this study are limited in the NASS-PCDS database and do not necessarily represent the overall US pedestrian crash statistics relating to the frequencies of types of pedestrian accidents and the percentage of related injuries. One of the NASS-PCDS variables, 'Vehicle pedestrian interaction (variable 524)', indicates the post-crash pedestrian kinematics. There are 17 codes to describe the types of interaction [4]. Four of those codes are picked out in accordance with frequencies of occurrences. They are categorized as following the four main types (Table 1).

The numbers of cases for each type are indicated in the fourth row of the table, the next two rows show the average pedestrian height, the average impact speed and its standard deviation. On the basis of this basic statistical information, a human FE model simulation, as shown in the last row, was carried out to verify the kinematics for corresponding types of impact. From the simulation results, corresponding to four different (Type A–D) kinematical modes, which is observed in Table 1.

Type A differs from the other three types in the relative velocity after impact. The Type A pedestrian is accelerated in the same direction in which the vehicle is traveling. The pedestrian's body is thrown forward in front of the vehicle.

In the other three types, Types B, C and D, the pedestrians are accelerated by the impact, up to a speed not more than the traveling speed of the vehicle. The torso of the pedestrian travels relatively backward with respect to the front end of the vehicle.

Table 1 Classification of vehicle–pedestrian interaction (Type A–D) in frontal crash

Variable	Type A	Type B	Type C	Type D
	5	1	2	4
Description in NASS-PCDS manual	Thrown straight forward	Carried by vehicle, wrapped position	Carried by vehicle, slid to windshield	Passed over vehicle top
(a): No. of pedestrian (total 275 cases)	35	82	138	20
Average pedestrian height [cm]	158	163	168	172
Average impact speed [km/h]	19.8	21.9	41.0	66.7
(standard dev.)	(12.2)	(11.2)	(19.6)	(10.5)
(b): MAIS 2–	25	67	60	4
(c): MAIS 3+	10	16	78	16
Ratio of MAIS 3+ (c)/(a) (%)	28.6	19.5	56.5	80.0
FE verification with adult male and 6-year-old child based on JAMA model				

Fig. 1 Components of four types of pedestrian crashes without outliers (refer Fig. 2)
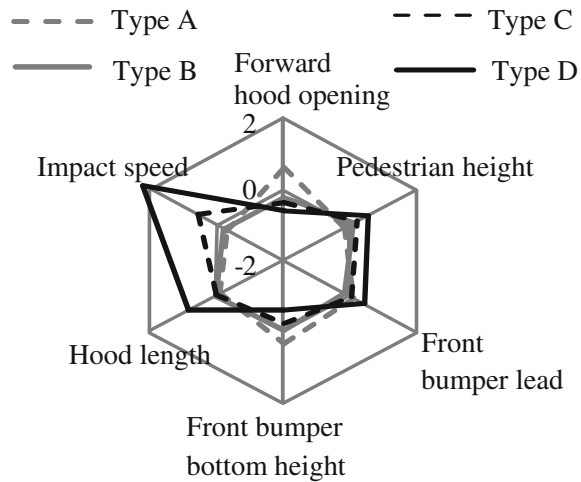
3 Characteristics of Vehicle–Pedestrian Interaction

Six-principal components characterize most of the features of the vehicle–pedestrian interactions as mentioned in [4]. Figure 1 shows the average values for each of the groups of four vehicle–pedestrian interaction types, related to those six principal factors, excluding the outliers (i.e., those data corresponding to higher impact speed V > 80 km/h as shown in Fig. 2). It is observed that:

Type D: The polygon shape in the radar chart corresponding to Type D is quite different and is separated from the others. It is more prominent on the *'Impact speed'* axis. However, note that the occurrence value of Type D is the lowest of the four, i.e., 20 out of 275 as mentioned in Table 1. Hence, the average contains more biases than the others.

Type A: The polygon in the radar chart corresponding to Type A plot gets separated from the other three types on the 'Forward hood opening', 'Front bumper bottom height' and 'Pedestrian height' axes. That means vertical height is the determining factor contributing Type A kinematics which include children.

Type B, C and D: The 'Impact speed' axis mostly represents the differences among Types B, C and D. It is to be noted that the three lines cross the 'Pedestrian height' axis in the same order and the 'Front bumper-bottom height' axis in the reverse order. Hence, the relative values of 'Pedestrian height' and 'Front bumper-bottom height' are closely coupled and inversely related influencing the post crash kinematics of the pedestrian.

Type B, C and D: The three types are nothing but an extension of a series of similar kinematical movement, distinguished by the amount of movement of the pedestrian moving backwards with respect to the front end of the vehicle. The four factors, 'Impact speed', 'Pedestrian height', 'Forward hood opening' and 'Front bumper bottom height' make the differences of the degree of backward movement.

Fig. 2 NASS-PCDS data plotted in impact speed versus height ratio h_p
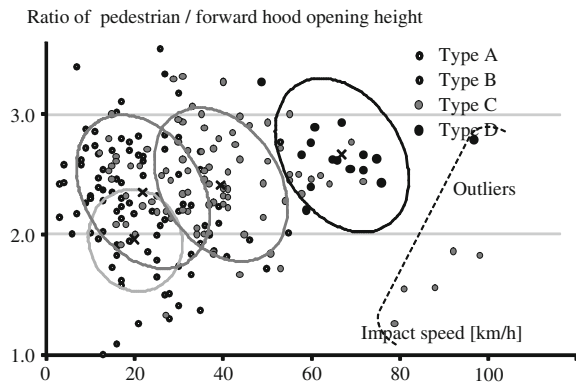
However, the result of the principal component analysis shows that the 'Forward hood opening' and 'Front bumper bottom height' are highly dependent, so the first principal component 'Forward hood opening' is chosen for further discussion.

The NASS-PCDS cases are plotted and clustered on the graph according to the kinematics types (Fig. 2). The horizontal axis indicates impact speed. The vertical axis shows the relative height ratio h_p of the pedestrian and the forward hood opening height. Four ellipses on the graph indicate typical contour lines (MD = 1) of the equivalent Mahalanobis distance (MD) of each type groups, and the cross marks 'x' on those four ellipse centers are the average values of the corresponding groups.

The distributions of the four types show dependency on the impact speed and height ratio. Types A and B share the same impact speed range, V < 41 km/h, although the height ratio of Type A is generally lower than Type B. With increase of impact speed V and height ratio h_p, ratios of Types B, C and D increase in turn. Impact speed range of V < 61 km/h consists of Type A, B and C. Shorter pedestrians tend to be Type A, while taller pedestrians fall into Type C. Type D plots increase their number in the speed range V > 60 km/h.

Type B, C and D ellipses have slightly negative inclinations. At the same impact speed and hood opening height, the negative inclination indicates that for relatively taller pedestrians (i.e., high h_p) the probability to be included in or falling into the next severe category (i.e., B-to-C or C-to-D) increases compared to that for relatively shorter pedestrians (i.e., low h_p). The same is true for relatively lower hood opening (i.e., high h_p) with the same impact speed and pedestrian height compared to that for relatively higher hood opening (i.e., low h_p).

These plots indicate that, '*Impact speed*', '*Pedestrian height*' and '*Front bumper—top height*' are the three most decisive factors to distinguish or classify the frontal post-crash pedestrian kinematics. As previously mentioned, h_p, the relative height of pedestrian with regard to vehicle front end is one of the main contributing factors that affect post-crash kinematics. Finite element analysis is introduced to show the differences between Type A and B pedestrian kinematics.

Table 2 Overall FE model dimensions and spinal chord model (a, b, c) with response identification (Figs. 3, 4)
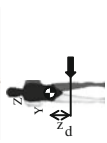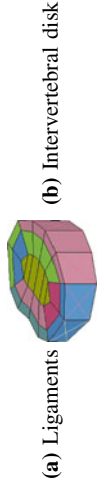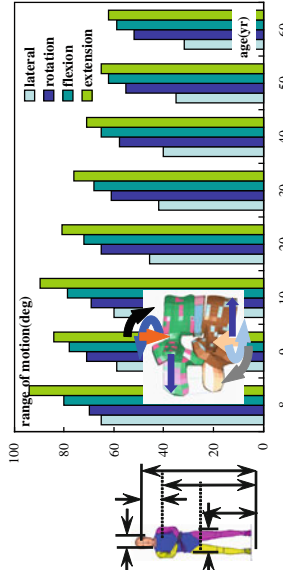
	Adult	Child	Spinal cord modeling (e.g., L3–L4)
Height	172 cm	120 cm	Spinal bones joined by different ligaments and intervertebral disk
Weight	71.9 kg	24.5 kg (range 20–32 kg)	European 6YO child 50th %-ile [7]
			(a) Ligaments (b) Intervertebral disk (c) Assembly is subjected to different modes of load
Input offset d_z	$d_z = 586$ mm	$d_z = 273$ mm	All parts scaled properly
IXX	11.8 kg m^2	1.67 kg m^2	Tension, bending, shear, torsion responses are tuned to match component level test results for adult [13] and also overall range of motion [9] which vary with age

Fig. 3 Component level response identification for torsional loading (quasi-static test)
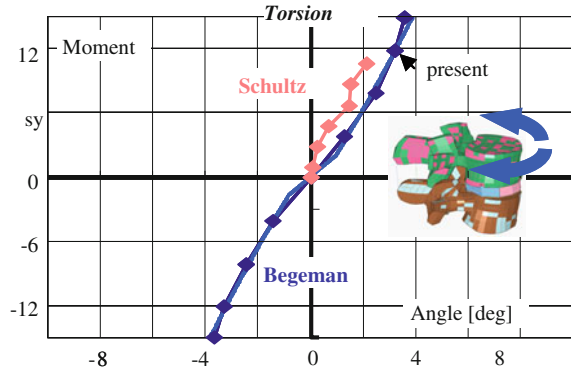
4 FE Analysis of Human Model

The findings from the NASS-PCDS database analysis match previous studies, as is mentioned in the previous section. In this section, we focused on some other aspects of head trajectory and head impact point, with the help of our human FE model. The findings of our study also match the NASS-PCDS database analysis.

An adult male pedestrian model was developed by Japan Automobile Research Inst (JARI) under the supervision of Japan Automobile Manufacturers Association (JAMA) in 2010 [5, 6]. The post-crash pedestrian kinematics, including head trajectory, are already validated with PMHS experiments [5, 12]. In this paper, the head Center Of Gravity (COG) trajectory of the pedestrian FE model is discussed. The adult model was modified in-house to create a 50th percentile 6YO child FE model based on European database of child anthropometry.

In Table 2, overall dimensions are given on the top left side. The adult 50th % ile adult male model is developed in the JAMA human model consortium. All parts of the 6YO child FE model are geometrically scaled according to the European children anthropometry data from this adult model [3, 7].

The weight 24.5 kg of the scaled model is the average of 6YO child weight margin of 20–32 kg. The impact point of the bumper is shown by an arrow. The overall modeling of the L3–L4 spinal chord region is shown in (a) ligaments are modeled by tension-only bar elements, (b) inter-vertebral disk: between two adjacent vertebra 2-layers and in the radial direction 3-layers of solid elements with various sets of material properties to simulate the different bending properties in frontal and lateral directions.

The assembly of L3–L4 is subjected to different types of loads to identify the basic behavior of response of the FE model as reported by JARI report in the JAMA human model consortium to match coupon tests of spinal chord carried out by Begeman and Schultz [10, 11]. Two main modes of response for pedestrian impact simulation are given in Fig. 3 for torsional behavior and in Fig. 4 for lateral bending behavior which are influential to pedestrian head impact time (HIT) on the hood and the distance the point of impact on the hood is from ground (WAD).
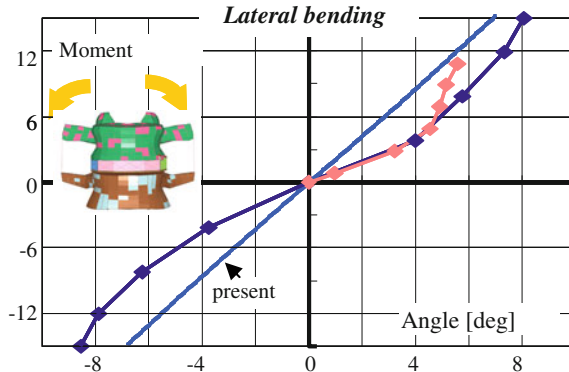
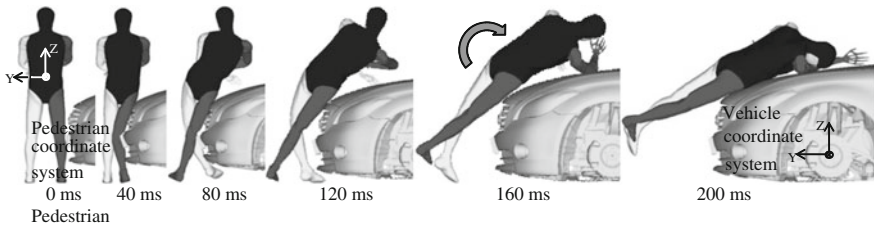**Fig. 4** Component level response identification for lateral bending modes of loading (quasi-static test)

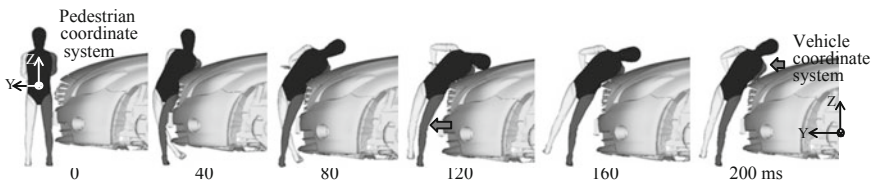**Fig. 5** FE analysis of an adult human (male) verus a sedan crash (V = 20 km/h)

Fig. 6 FE analysis of a child human (6-year-old) versus a sedan crash (V = 20 km/h)

The graph inside (c) shows the change in range of flexibility with age, with younger children being relatively more flexible than adults.

Adult-male: In Fig. 5, the adult-male human model is hit at his anterior lower leg by the bumper, and falls down to the hood. In the initial phase (0–80 ms), the head moves in the Y-axis direction (the vehicle coordinate system), until his upper femur gets constrained by the front edge of the hood. Then the upper body and the neck moves like a duplex pendulum, rotating around the local X axis of the pedestrian coordinate system as shown in the middle of Fig. 7.
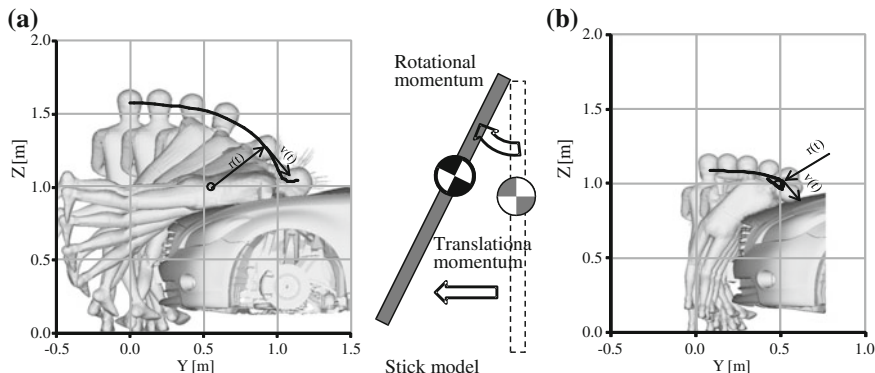
Fig. 7 Superimposed animations of an adult and a child FE models **a** Adult male kinematics (0–280, 40 ms interval) **b** Child kinematics (0–120, 20 ms interval)

6-year-old child: Figure 6 is the 6-year-old child pedestrian model. He was hit right under his COG, and is accelerated in the positive Y direction in the global system, the same as the traveling direction of the vehicle. The pedestrian body is accelerated to a velocity higher than that of the vehicle and his body is gradually thrown forward (160 ms). In this case the upper body of this child pedestrian is lifted up after hitting his abdomen against the front edge of the hood. His head COG trajectory (Fig. 7b) draws an arc centering at the bumper (R1) before his upper body is constrained by the hood. Then his upper body rotates around the front hood edge (R2). After his shoulder contacts the hood (80 ms), the head COG rotates around his neck (R3). At this time (80 ms), his body COG gets accelerated in the positive Y direction and starts to move away from the vehicle.

Figure 8a, b is the time histories of the tangential velocity v(t) of the head COG and the rotational velocity θ(t), respectively. The rotational velocity θ(t) is calculated from the tangential velocity v(t) and the curvature radius r(t) of the head COG trajectory.

$$\theta'(t) \ = \ v(t)/r(t) \tag{1}$$

The curvature radius r(t) is calculated by the smoothed trajectory of the head COG (Fig. 7). The resultant translational velocity of the head COG (Fig. 8a) of the child FE model hits its highest value when its torso contacts the car front and the head starts to fall down (45 ms). The same for the adult model is much later at 110 ms. The maximum value of the resultant velocity for the child model is slightly lower than that of the adult model. However, the calculated angular velocity (Fig. 8b) for the child and the adult models show quite different patterns. The angular velocity of the adult model (black line) takes its first local maximum 12.9 rad/s at 160 ms when the curvature center of the head COG trajectory comes around its pelvis. The second local maximum at 230 ms (the black dashed line) is the time when the head contacts the hood. The angular velocity of the child model shows a peaky curve. The second largest peak 85.3 rad/s at 80 ms appears when
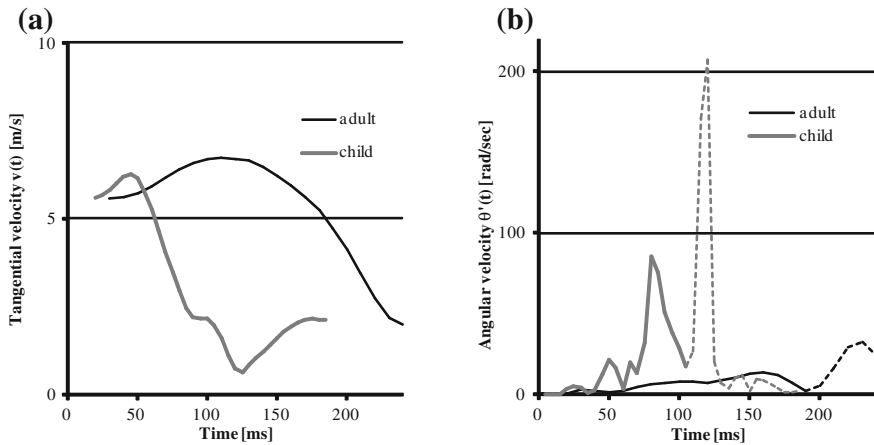
Fig. 8 Head velocity of adult and child FE models (20 km/h without braking) **a** Resultant translational velocity **b** Angular velocity

the child's shoulder is constrained by the hood and the head COG rotates around its neck. The maximum peak at 120 ms appears at the time of the head-hood contact. Contact to the hood bends the head trajectories and minimizes curvature radius. Thus, the highest peak is caused by graphical definition. The following discussion is for the second largest peak.

The tangential velocity v(t) of the adult head COG is 5.9 m/s at the time when the angular velocity takes its secondary peak at 160 ms. The counterpart of the child head COG is 2.9 m/s at 80 ms, less than the half of that of the adult. The angular velocity peak of the head COG is derived from the curvature radius of the trajectory and is dependent on the height ratio.

5 Ground-to-Head-Contact Distance

The measurement of ground to head contact point, i.e., wrap around distance (WAD) from PCDS database is plotted in Fig. 9. The value of ground to head contact point, i.e., wrap around distance (WAD) and the ratio of the WAD/pedestrian height of FE simulation results are plotted for 6YO child pedestrian simultaneously in Fig. 10. In general, the ratio of the WAD/pedestrian height values (children: less than 1.0, adults: greater than 1.0, [8]), agree well with present FE simulations.

Figure 11 show the head COG trajectories of an adult male FE analysis of a crash case with a sedan traveling at 20 and 40 km/h. Comparing the constant velocity cases (black thin lines), the head contact point for the moderate speed (40 km/h) case, locates 220 mm rearward compared to that of the relatively low speed (20 km/h) cases. The difference in head contact point matches the value

Fig. 9 Ground-to-head-contact distance versus impact speed (*gray-line* with braking, *thick-line* without braking (adult)
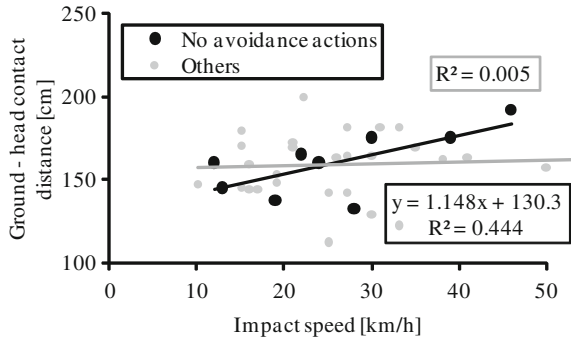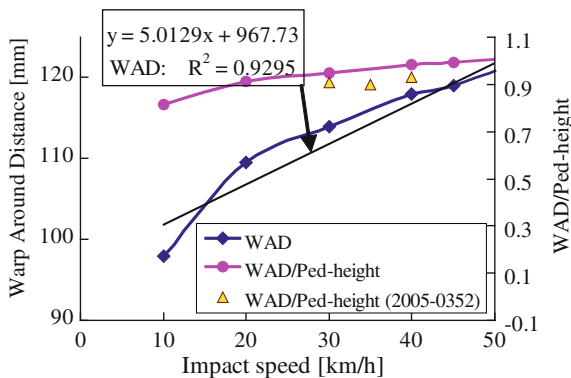

Fig. 10 Warp around distance (WAD), height WAD/pedestrian height versus speed (6YO, hp = 1.5)

derived from the approximated relation as shown in Fig. 9, where 1.148 is the gradient of the ground-to-head-contact distance without braking and steering cases, with respect to the impact speed, as calculated below by Eq. (2).

$$1.148 \times \Delta v = 1.148 \times 20 = 22.9 \text{ [cm]} = 229 \text{ [mm]} \qquad (2)$$

In both Fig. 11a, b, the trajectories of deceleration (braking) cases go forward of the vehicle after contacting the hood. In these cases, deceleration switches the pedestrian kinematics from Type C to Type B category, and it may reduce or affect the risk of head-windshield injury in case by case. It is interesting to note that the gradient of WAD with respect to the impact velocity is four times higher for children (5.01) than adults (1.148). It is also very clear that the gradient of WAD at low impact velocity V = 10–20 km/h is stiffer than in the region above V > 20 km/h because of the low value of the pedestrian and hood height ratio h_p. This is similar to the tendency as observed in Fig. 2 from PCDS data. Present FE simulations results are well supported by actual accident field data. The three GIDAS cases, closest to our simulation, are chosen from Ref. [8, 2005-0352] and poltted in Fig. 10 as triangular marks estimated from Madymo simulation for comparison.
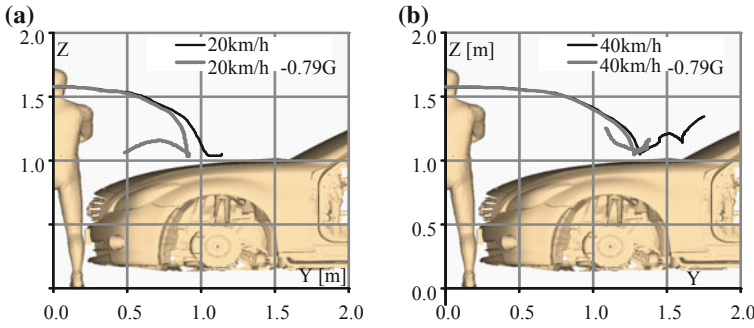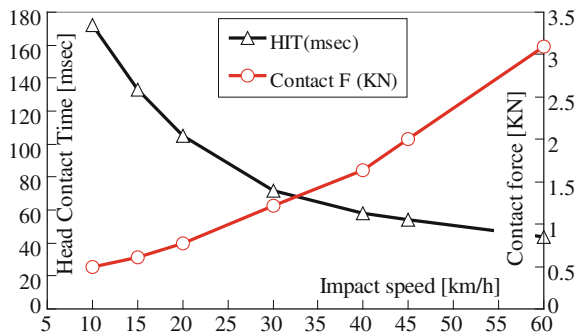
Fig. 11 Head COG trajectory, with/without vehicle deceleration at V = 20, 40 km/h. **a** Initial velocity 20 km/h, **b** Initial velocity 40 km/h


Fig. 12 Head impact time (HIT) and contact force F versus impact speed V (6YO pedestrian hp = 1.5)

They are slightly lower than the present FE model values. This can be well explained by the fact that the 3D detailed FE model based post-crash kinematics simulates more closely the flexible and damped overall dynamic movement of human pedestrians than that of the lumped-mass Madymo model simulation and consequently more likely to match the field accident data with higher accuracy. It should be noted that the order of magnitude and the point of change of the gradient of WAD are dependent on the frontal geometry of the vehicle.

Figure 12 shows the variation of head contact time and contact force F exerted on the head of 6YO child from the hood for different speeds of impact. At lower speed of impact (V < 20 km/h), the gradient of the "increase of the head contact time" is more than that of the "decrease in head contact force F" with decrease of impact speed. It is partially due to the low tangential velocity and large rotation for 6YO child head at low speed of impact just before contact as explained in the previous section. This is not observed in case of adults. As mentioned in Ref. [8], GIDAS and also the PCDS accident data both indicate that for AIS + 2 injuries, percentage of AIS + 2 head injuries for children (56 %) is almost two times than that of the adult (31 %) even though the overall average speed of impact of head for adult is 10–15 km/h higher than that of the children. Large rotational velocity

Fig. 13 Comparison of head trajectory w.r.t speed V = 60, 30 k/h and hp = 1.5, 1.55 for 6YO pedestrian
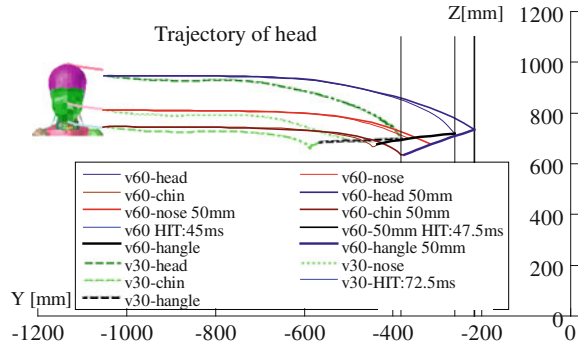
with respect to torso just before the head contact with the hood together with low tolerance level of injury are two possible influencial factors. However, further investigation is necessary with advanced FE head injury model to study in detail about the minute mechanism of head injury in the future.

Figure 13 shows the comparison of head trajectories for two different speeds of impact (60, 30 km/h) and the sensitivity of pedestrian height versus hood height ratio hp (1.5 and 1.55, 50 mm difference in height) for a 6YO pedestrian. Three sets of trajectories are plotted corresponding to the target marks fixed to (i) the top of head, (ii) the tip of nose and (iii) the bottom of chin with additional three vertical lines on Y-axis indicating the end points at the time of contact on the hood in vehicle co-ordinate system. The line joining the head, nose and chin positions at the time of impact in Y–Z plane indicates the angle of head impact on hood. With the increase of relative height ratio hp, 1.5–1.55 (i.e., relatively 50 mm taller pedestrian or 50 mm shorter hood opening), the head impact time HIT is increased by 6 % (45–47.5 ms) at V = 60 km/h but the head impact angle (v60-hangle-50 mm) is decreased. The change in HIT at V = 45 km/h is about 13 % but not plotted in this graph. Again, at low impact speed V = 30 km/h, the WAD value is reduced by 130 mm but the head impact angle (v30-hangle) is increased, almost horizontal i.e., 90 degrees of rotation of head. As the inertia of the pedestrian upper body about the horizantal plane at the height of hood opening, is proportional to the square of the distance of COG of the upper body (refer Table 2), the time and the distance of flight of head are highly sensitive to hp.

6 Conclusions

This paper systematically discussed the main determining factors of post-crash pedestrian kinematics on the basis of a detailed study on NASS-PCDS. Those cases are categorized into four types (Type A–D) of post-crash pedestrian kinematics. In conclusion, post-crash pedestrian kinematics is determined mainly by impact speed, deceleration due to braking and pedestrian-vehicle height ratio.

These findings were verified and endorsed by a Human FE model. The study is summarized as follows:

Type A: Type A occurs at impact speed V < 41 km/h. Shorter pedestrian height and higher forward opening height of vehicle lead to Type A kinematics. Shorter pedestrians tend to be thrown forward and are likely to be categorized as Type A. When the impact point is higher than the pedestrian COG, the maximum part of the crash impulse is converted to translational momentum rather than rotational. The translational momentum turns into the positive longitudinal velocity.

Type B: The Type B category shares the lower range of impact speed with Type A, although Type B mainly consists of taller pedestrians. An impact point below pedestrian COG produces rotational momentum, and therefore the proportion of the translational momentum is reduced. The pedestrian moves at a lower velocity than the vehicle, sliding on the hood.

Type C: Type C cases exceed Type B cases at the impact speed of 31–40 km/h. Type C group has a higher ratio of MAIS3 + injuries. Taller pedestrians tend to fall into Type C cases at the same impact speed. Deceleration of the vehicle may reduce the chance or risk of head injury.

Type D: Type D cases occur at the impact speed range higher than 60 km/h. In these cases, after pedestrians' lower extremities contact the frontal area of vehicles, their heads are most likely to directly contact the windshields without their head contacting to the hoods at all.

Head injury: The tangential velocity v(t) and the rotational velocity θ'(t) are calculated from the trajectory of the head COGs for both the adult and the child FE models. Although the maximum value of the tangential velocity for the child head COG is slightly lower than that of the adult head COG, the maximum value of the rotational velocity for the child head COG is double that of the adult head COG. Relative height of the pedestrian and the vehicle hood edge, as well as the impact speed and braking, determines the head trajectory.

Ground-to-head-contact distance: The continuous distance from the head contact point to the ground surface, measured along the vehicle surface, depends on the impact velocity, pedestrian height and the front hood opening height. Higher impact speed makes the ground-to-head-contact distance longer and consequently leads to higher head-windshield injury risk. FE analysis results quantitatively support the past published literature. The ground-to-head-contact distance dependency on the impact speed is numerically verified by FE analysis.Detailed human FE analysis is essential to reconstruct crash cases correctly and to better articulate hidden information in accident databases. Kinematics of child is different from adults.

References

1. Mizuno Y (2005) Summary of IHRA pedestrian safety WG activities. ESV 19 No. 138
2. Longhitano D et al (2005) Influence of vehicle body type on pedestrian injury distribution. In: SAE world congress
3. Serre T et al (2010) Child pedestrian anthropometry: evaluation of potential impact points during a crash. Accid Anal Prev 42(6):1943–1948
4. Kawabe Y (2012) Different factors influencing post-crash pedestrian kinematics. In: SAE world congress 2012-01-0271
5. Takayama S et al (2011) The clarification of individual injury mechanism difference in pedestrian FE model utilizing cadaver scaling and posturing techniques. ESV 22 No. 11-0414
6. Ejima S et al (2003) Modification and validation of human neck model under direct head loading. ESV 18 No. 333
7. Serre T et al (2009) Comparison between new data on children anthropometry and CRS dimensions. ESV 21, paper 09-0484
8. Yang J et al (2005) Correlation of different impact conditions to the injury severity of pedestrian real world accidents. ESV 19 paper 05-0352
9. Caris TL et al (2006) Cervical range of motion data in children. SAE 2006-01-1140
10. Schultz AB et al (1979) Mechanical properties of human lumbar spine motion segments part-I. Trans ASME 101:79–84
11. Begeman PC et al (1994) Visco-elastic shear response of the cadaver hybrid III lumbar spine. In: SAE world congress 942205
12. Nishimura R et al (2002) Development of the human FEM model for child pedestrian. JSAE spring convention, 20025504
13. Martin RB et al (1977) Age and sex-related changes in the structure and strength of the human femoral shaft. J Biomech 10:223–231